Supporting Information

Keng et al. 10.1073/pnas.1117566109

SI Text

Instrumentation. ***EWOD chip fabrication.*** The EWOD chips consisted of two plates: one base plate with defined electrodes to route, heat, and measure temperature of droplets, and a cover plate with a conductive layer to ground droplets for electrowetting (Fig. S1). The base plate was fabricated from a 700 μm-thick glass wafer coated with 140 nm of indium tin oxide (ITO) (Semiconductor Solutions LLC). 20 nm of chrome and 200 nm of gold were evaporated onto the wafer and 1.6 μm photoresist was spin-coated onto the gold. Photolithography was used to selectively remove the metal layers (gold, chrome, and ITO) by wet etching for patterning EWOD electrodes, heaters, connection lines, and contact pads. Another photolithography step followed by wet etching was used to selectively remove the top two metal layers (gold and chrome) from the EWOD electrodes and heaters for defining the connecting lines. A 1 μm dielectric layer of silicon nitride was deposited by plasma-enhanced chemical-vapor-deposition (PECVD), and 1 μm of Cytop® was spin-coated and annealed at 200 °C to make the surface hydrophobic. The cover plate was prepared from an essentially same wafer as the base plate—700 μm- thick glass wafer coated with 150 nm of ITO (Delta Technologies Inc.). The wafer was coated with thinner layers of silicon nitride (100 nm) and Cytop® (100 nm) than the base. The cover plate was spaced and bonded to the base plate at its corners using two layers of double-sided tape (3M Inc.), each listed as 100 μm thick but measured to be about 70 μm thick.

Unit operations on EWOD chip. Chemical syntheses on the EWOD chip are performed by executing sequences of fundamental unit operations (Fig. S2):

- Transport: The reaction site is filled with reagents by pipetting reagent droplets (volume 2–4 μL each) to the reagent loading sites then actuating series of electrodes to transport these droplets to the center of the chip (Fig. S2 *A* and *B*). Generally, several reagent droplets must be loaded sequentially to fill the reaction site (maximum volume ∼17 μL).
- Mixing/Redissolution: Gentle heating accelerates mixing of newly loaded reagents with previous contents of reaction site (Fig. S2*C*).
- Reaction: The reaction site is heated to perform a chemical reaction within the previously mixed droplet (Fig. S2*D*).
- Evaporation: Solvent is evaporated by heating the liquid at the reaction site while simultaneously blowing a stream of inert gas past the droplet surface (Fig. S2*E*).

EWOD heater temperature controller. The multichannel heater controller and driver were designed to provide an expandable platform for achieving and maintaining multiple, independent EWOD reaction sites at precise temperatures, including segmented heaters for spatially varying temperature profiles (e.g., the concentric ring pattern), or heaters on different chips. The instrument was specifically designed for the resistive micro-heaters patterned on the EWOD chip. The controller incorporates a low noise, real-time, zero-resistance current measurement, and amplification while providing a self-powered, amplified heater driver with parameters that can be controlled by dedicated software.

The heater output voltage V_t^{out} was given by:

$$V_t^{\text{out}} = \max(0.35, \min(20, V_{t-1}^{\text{out}} + \Delta V)).$$

A multiband proportional gain control algorithm was designed to achieve speed and stability for temperature control. The voltage change was limited to a maximum range of +1 and −1V to avoid destabilization in case of extreme temperature set-point or an erroneous reading.

$$\Delta V = \max(-1, \min(1, K(T_{\text{set}} - T_t)))$$

$$K = \begin{cases} 1/50 & \text{for } |T_{\text{set}} - T_t| \geq 40 \\ 1/20 & \text{for } 5 \leq |T_{\text{set}} - T_t| < 40 \\ 1/10 & \text{for } |T_{\text{set}} - T_t| < 5 \end{cases}.$$

Temperature of any heater time t is given by T_t:

$$T_t = \frac{\left(\frac{V_{t-1}^{\text{out}}}{I_t} - R_{\text{RT}}\right)}{\frac{dR}{dT}}.$$

R_{RT} is the resistance at room temperature measured with an application of 350 mV which applied less than 100 μW causing less than 2 °C temperature change. The 350 mV applied potential set a baseline of current measurement which was well above the absolute accuracy of the system for all heaters. The <2 °C temperature change along with room temperature variations were the determining factors in the absolute accuracy of the temperature control system. Temperature measurement resolution once an experiment had started was better than 0.1 °C.

$\frac{dR}{dT}$ is the change in heater resistance with temperature which was calibrated for each heater in an oil-bath and shown to be constant over the range of temperatures used in this experiment. I_t is the current obtained in the interval between V_t^{out} and V_{t-1}^{out} which usually lasted 100 ms.

$$I_t = \frac{\sum_{(t-1)+20\text{ ms}}^{t} I_t}{n} - I_{\text{bias}}.$$

Current acquisition in this interval was triggered with the voltage change from the control program. Acquisition was at 5,000 samples/s for each heater and the first 20 ms of data was discarded to allow stabilization of heaters and resistive-capacitive (RC) time constants from stray capacitances and low pass filters in the acquisition hardware. Current acquisition was performed with a zero-resistance transimpedance amplifier incorporating an integrated antialiasing filter with a 1 ms time constant and an output of 100 mV/mA. The current monitor circuits for each heater were designed in house and packaged with a multi heater driver, capable of providing 4× amplification of driving signal (Vout) and up to 20 V and 50 mA to each heater. The driver was controlled by the analog output of a DAQ card (NI USB-6259, National Instruments) and the current monitor signal was acquired with a 16-bit analog-to-digital (A/D) converter from differential inputs of the same device. The current data was averaged over each acquisition interval to eliminate 60 Hz and other circuit noise while the bias current I_{bias}, obtained from the circuit under zero applied potential was subtracted from this value.

Cerenkov imaging. The technique of Cerenkov imaging for measurement of quantity and distribution of radioactivity in microfluidic chips has been described previously (1). As an enhancement, the system was modified to enable switching be-

tween a camera for Cerenkov imaging and another camera for bright-field imaging to allow separate optimization of image requirements (Fig. S5). The setup is enclosed in a light-tight enclosure (Hoffman CSD20168) to eliminate the effect of ambient light on Cerenkov image quantification. A servomotor (Hitec HS-485HB) was used to rotate a first surface mirror (Techspec) 45° from parallel with the chip towards either camera for Cerenkov imaging or video monitoring. A Sony ICX098BQ progressive scan CCD (Imaging Source DFK 21AU04) coupled to a variable focal length lens (MC Electronics 5.0–50 mm) was used to monitor droplet movement on the EWOD device. A slow scan cooled Kodak KAI-04022 CCD (Quantum Scientific Imaging 540) coupled to a fixed focal length lens (Nikon Nikkor 50 mm) was used to assess the radioactive distribution throughout the synthesis process via Cerenkov emission. In order to preserve the quantitative reliability of the Cerenkov imaging camera, the CCD was kept at a fixed distance away from the EWOD chip. Furthermore, a lead brick was placed between the chip and the CCD to reduce the number of direct interactions of the 511 keV photons with the CCD. The Cerenkov camera body was fixed to the outside of the light-tight enclosure in order to (*i*) maintain reproducible distance between the camera and chip and (*ii*) to allow ventilation for camera cooling. The Cerenkov imaging camera's field of view was set to be approximately 5×5 cm, slightly greater than the dimensions of the EWOD chip. Exposure time was set to 30 s. Temperature was set to −10 °C to reduce dark current.

Optimization of Radiolabeling Reaction on Cytop-Glass Substrate. Although the optimal conditions for the radiosynthesis of [^{18}F]FDG have been well established at the macroscale, radiosynthesis at the microscale has yet to be thoroughly investigated to understand the effect of differences in the reaction geometry, surface-to-volume ratio, reaction scale, as well as heat and mass transfer in the microfluidic chips. We investigated the optimal radiolabeling condition within microliter volume droplets on Cytop-coated glass substrate to achieve high and reproducible fluorination efficiency. Cytop-coated glass substrates have comparable surface chemistry and geometry to the full EWOD chip, but are much easier to fabricate, enabling high throughput optimization reactions to be performed. Typically, the [^{18}F]fluoride was dried on an open, heated Cytop-coated glass substrate. During the fluorination step, a Cytop-coated glass cover plate was placed on top of the reaction droplet (with a gap height 150 μm using two layers of 3M double-sided adhesive) to mimic the sandwiched droplet configuration on EWOD. We have also designed a heating platform made of an aluminum block with 15 mm × 20 mm area to achieve comparable heating region as on EWOD chip (~12 mm diameter heater). For all of these Cytop-glass experiments, the heating block set-point was calibrated on the upper surface of the glass slide using an external thermocouple to ensure that the surface temperature used in these optimization reactions is comparable to the surface temperature measurements from integrated electrodes within the EWOD chip. Based on this reaction setup, we investigated the effect on the fluorination efficiency of (*i*) concentration of the phase transfer catalyst and the precursor solution, (*ii*) reaction temperatures and times, and (*iii*) droplet to heater size ratio. In each of the optimization studies described in the next several sections, 3–5 experiments were performed for each data point (summarized as average and standard deviation of radiolabeling efficiency). The modified synthesis of [^{18}F]FDG was performed in DMSO (a high boiling point, aprotic solvent with $b.p. = 182$ °C) to overcome the uncontrolled evaporation of MeCN on the open EWOD platform. This critical modification in the chemistry enabled systematic screening of reaction conditions as it helped decouple the relationships among concentration, reaction temperature, and droplet lifetime when using MeCN.

Effect of concentrations. The concentrations of Kryptofix, K_2CO_3 and mannose triflate were first investigated on Cytop-coated glass substrate while keeping the reaction temperature and time constant at 100 °C and 5 min, respectively. In our first attempt, typical radiosynthesis conditions used in the conventional macroscale synthesis were directly translated onto EWOD chip by simply reducing the reaction scale while keeping the concentrations of the reagents to 12 mM, 6 mM, and 11.5 mM of Kryptofix, K_2CO_3, and mannose triflate, respectively (2, 3). As illustrated in Fig. S3*A* (blue color), the average conversion efficiency of FTAG was only 50.8%, which is below the average conversion obtained in the macroscale radiosynthesis (typically >80%). Upon increasing the concentration of Kryptofix, K_2CO_3, and mannose triflate to 126 mM, 61 mM, and 104 mM, we observed a significant increase in the fluorination efficiency, to a value comparable to conventional radiosynthesis. It is unclear why the two reaction scales have such disparate optimal concentrations. Investigations showed that higher concentration of precursor is critical in achieving higher conversion, while concentrations of Kryptofix and K_2CO_3 seem to be less important. We did observe that increasing the Kryptofix concentration from 12 to 28 mM was found to improve the *repeatability* of conversion efficiency from $79 \pm 12\%$ ($n = 2$) to $86 \pm 6\%$ ($n = 7$). While our intention was not to perform exhaustive studies, these preliminary studies provided guidelines for selection of concentrations and conditions for subsequent studies.

Effect of reaction temperature. Due to the high boiling point of DMSO used in this synthetic strategy, a wide range of temperatures could be investigated while keeping other reaction parameters constant. Three different temperatures (82 °C, 100 °C, 120 °C) were explored for the radiolabeling of mannose triflate in DMSO based on the optimized reagent concentration (see *Effect of concentrations*) and constant reaction time of 5 min. Fig. S3*B* shows that high fluorination conversions were only achieved at temperatures above 100 °C.

Effect of reaction time. The kinetics of the radiolabeling reaction performed within the confined microliter droplet were determined to achieve the shortest synthesis time. In this set of experiments, both the 1 min and 7 min reaction times were performed once ($n = 1$), while the experiments at reaction time of 3 and 5 min were repeated 3–5 times. As shown in Fig. S3*C*, the conversion efficiency increased steadily starting at 1 min and began to plateau at 5 min. We have also explored higher temperature radiosynthesis at 120 °C to increase the conversion efficiency at 3 and 5 min. At higher temperature, an increase of collision frequency between reactants could be attained, thus resulted in an increased in the conversion efficiency from 60% to 75% for the 3 min reaction. However, less significant improvement (+4%) was observed for the 5 min reaction as most of the reactive, [$^{18}F^-$]KF/$K_{2.2.2}$ has reacted over the 5 min period. During the initial implementation of these optimized reaction conditions (concentrations, temperature, and time) onto the EWOD chip, we found that the fluorination efficiency at 120 °C increased by an additional 10% when the labeling reaction was performed for 10 min vs. 5 mins. Thus, we continued to perform the radiolabeling reaction for 10 min in subsequent experiments.

Droplet to heater size ratio. The optimal reaction droplet size and volume loaded onto EWOD chip were explored to achieve highest radioactivity and conversion efficiency based on our first generation EWOD chip with 1 mm × 1 mm multifunctional electrode. These studies confirmed that the highest fluorination efficiency was attained with droplet to heater size ratio approaching 1 (Fig. S4). Presumably, larger droplets experience a lower average temperature due to contact with both the heater region and

surrounding nonheated region, which results in slower reaction and reduced conversion. Based on these results, we optimized the chip and heater design to ensure uniform heating of larger droplets (to enable preparation of mCi amounts of [^{18}F]FDG).

Effect of nitrogen flow. A Gauge 30 needle was aligned parallel to the gap on the EWOD chip (indicated by the blue arrow) to provide nitrogen flow during the evaporation, drying and reaction steps. The nitrogen flows facilitates the removal of solvent vapor out of the chip, and thereby increasing the efficiency of the drying process. Fig. S6 shows the effectiveness of the nitrogen stream in removing the vapor condensation away from the reaction site. In the absence of nitrogen, vapor condensation accumulates surrounding the reaction droplet, thus decreases the rate of drying.

Cartridge Purification. Due to the desire to maintain the small volume for small animal imaging (e.g., <200 μL, formulated in saline for mouse injection), a custom-made, miniature purification cartridge was developed. Homemade cartridges for purification of [^{18}F]FDG were packed with cation exchange (5 mg AG-50W-X4, BioRad Laboratories) and ion retardation resin (5 mg, AG11 A8, BioRad) with 50–100 mesh size, neutral alumina (30 mg, particle size 50–300 μm, Waters) and C-18 (20 mg, particle size 55–105 μm, Waters) within a 750 μm ID perfluoroalkoxy tubing. The resins were sandwiched between two polyethylene frits (20 μm pore size). The crude reaction is first passed through a strong cation exchange resin (functionalized with sulfonic acid groups) to neutralize the acid used in the deprotection step. The second bed of resin is composed of both a weak cation and anion functional groups to trap any ionic species that remain in the mixture. The unreacted [^{18}F]fluoride ion is retained in the subsequent neutral alumina resin and finally the reaction mixture is passed through the reverse-phase silica (C-18 functionalized beads) to remove other organic impurities. The optimized purification cartridge for [^{18}F]FDG contained a total of 60 mg of resins packed inside a length of 1/16″ OD tubing (Fig. 3*B* of main paper), which is effective in removing acids, Kryptofix, unreacted [^{18}F]fluoride, and other organic impurities. The cartridge was first conditioned with ethanol (0.5 mL), followed by water (1 mL; 18 MΩ). The final product was eluted with 250 μL of water to achieve a 99% chemically pure [^{18}F]FDG and 88% purification efficiency.

Quality Control of [^{18}F]FDG Synthesized on EWOD. ***Radio thin-layer chromatography (radio-TLC).*** The radio-fluorination and hydrolysis efficiencies of [^{18}F]FDG were determined by TLC on silica gel plates, with a 95:5 (by volume) acetonitrile/water mixture as eluent. The radioactivity distribution was scanned with a γ-counter (MiniGITA star, Raytest). The retention factors (R_f) of [^{18}F]F$^-$, [^{18}F]FDG, and [^{18}F]FTAG were 0.00, 0.47 and 0.65, respectively. Upon purification of the crude [^{18}F]FDG that was extracted from the EWOD chip through the custom-made miniaturized cartridge, the radio-TLC of the final [^{18}F]FDG showed >99% radiochemical purity as shown in Fig. S7*A*. During the optimization studies of the hydrolysis reaction of the crude [^{18}F]FTAG to [^{18}F]FDG, the TLC plates were developed in a 50:50 (by volume) hexanes/ethyl acetate mixture. Under this condition, both the unreacted fluoride and fully hydrolyzed [^{18}F]FDG remained on the baseline, while partially hydrolyzed intermediates travel away from the baseline. Before arriving at our optimal hydrolysis protocol, partially hydrolyzed [^{18}F]FTAG was obtained as evidenced in the radio-TLC. For the red trace in Fig. S7*B*, the hydrolysis was performed in HCl (1N, 2 μL) and heated at 100 °C for 5 min. By instead performing hydrolysis at 100 °C for 10 min in a mixture of 1 N HCl and MeCN (50/50 vol/vol) (15 μL), complete hydrolysis was observed (blue trace).

Radio high performance liquid chromatography (radio-HPLC). Radio-HPLC on Phenomenex Luna reversed-phase C-18 column (250 × 4.6 mm), with isocratic elution of MeCN/H_2O 70:30 (vol/vol) at a flow rate of 1 mL/min of the final [^{18}F]FDG product was performed. The isocratic radio-HPLC (Fig. S8*B*) supports the radio-TLC results, in which other radiochemical impurities were not detected.

Gas chromatography for residual solvent analysis. A quantitative method for determining amount of residual solvents as well as the DMSO by-products in [^{18}F]FDG was developed using gas chromatography (Agilent 7890A) equipped with a flame ionization detector (FID), an auto sampler and a JW DB-WAX (polyethylene glycol) column (30 m long, 0.25 mm ID and a phase thickness of 0.25 μm). Fig. S8*A* shows a typical chromatogram of standard solutions of solvents and DMSO degradation products. The GC was operated in a helium flow of 2 mL/min, hydrogen flow of 30 mL/min and an air flow of 350 mL/min. In this method, the initial oven temperature was set at 30 °C and held for 2 min followed by a temperature ramp of 10 °C/min to 80 °C. After holding at 80 °C for 0.5 min, the temperature was ramped at 10 °C/min to 150 °C and held for 10 min to separate the mixtures.

Colorimetric Kryptofix test. To analyze the amount of residual Kryptofix in the final FDG product, we adapted a new quantification method developed by Kilbourn, et al. (4) In this method, the TLC plate was stained with potassium permanganate solution to visualize the oxidized Kryptofix (appears as a yellow spot). This method was chosen over the conventional iodine staining method recommended by the USP because this method provides higher sensitivity (down to 10 μg/mL concentration). The iodine staining method has additional disadvantages: it tends to lead to false reading for tracers containing nitrogen or the presence of added stabilizer. 4,7,13,16,21,24-Hexaoxa-1,10-diazobicyclo [8.8.8]hexacosane (Kryptofix $K_{2.2.2}$, 98%) was purchased from Aldrich and used as received. Standards Kryptofix solutions of 400 μg/mL, 40 μg/mL, and 4 μg/mL were prepared by dissolving Kryptofix in 18 MΩ water. TLC plates were spotted with 2 uL samples using a micropipette and the plates were stained using potassium permanganate in aqueous potassium carbonate solution. Stock potassium permanganate was prepared according to the standard laboratory procedure: potassium permanganate (3 g), potassium carbonate (20 g) and 5% sodium hydroxide (5 mL) were dissolved in water (300 mL). The spotted TLC plates were dipped into the stain solution, and the excess stain was absorbed onto a paper towel. The plates were dried using a heat gun at low heat. A yellow spot was observed on the TLC with all the Kryptofix standard solutions as low as 4 μg/mL. A series of control, Kryptofix standard solutions and FDG sample were spotted along the TLC plate to compare the visibility of the yellow spot. Semiquantitatively, the yellow spot from the FDG sample is less intense in comparison to the 4 and 40 μg/mL solution, which confirmed that the concentration of Kryptofix in the final FDG sample is below the allowable level (50 μg/mL) determined by the USP.

Comparison of Synthesis on EWOD vs. Other Microfluidic Platforms. To highlight the differences between the EWOD microfluidic platform presented here and other microfluidic platform, we summarize in Table S1 several parameters of FDG synthesis on EWOD with FDG synthesis on other reported microfluidic platforms. The other platforms are classified as "batch" approaches or "flow-through" approaches as described in the Introduction. For the PDMS batch approaches, there is some ambiguity in the precise meaning of reported results but we make our best judgement in summarizing them. For flow-through systems, we restrict our comparison to those that are microfluidic-chip based, and omit those based on capillary reactors.

1. Cho JS, et al. (2009) Cerenkov radiation imaging as a method for quantitative measurements of beta particles in a microfluidic-chip. *Physics in Medicine and Biology* 54:6757–6771.
2. Padgett HC, et al. (1989) Computer-controlled radiochemical synthesis: A chemistry process control unit for the automated production of radiochemicals. *International Journal of Radiation Applications and Instrumentation. Part A. Applied Radiation and Isotopes* 40:433–445.
3. Gomzina NA, Vasil'ev DA, Krasikova RN (2002) Optimization of automated synthesis of 2-[^{18}F]-Fluoro-2-deoxy-D-glucose Involving Base Hydrolysis. *Radiochemistry* 44:403–409.
4. Scott PJH, Kilbourn MR (2007) Determination of residual Kryptofix 2.2.2 levels in [^{18}F]-labeled radiopharmaceuticals for human use. *Applied Radiation and Isotopes* 65:1359–1362.

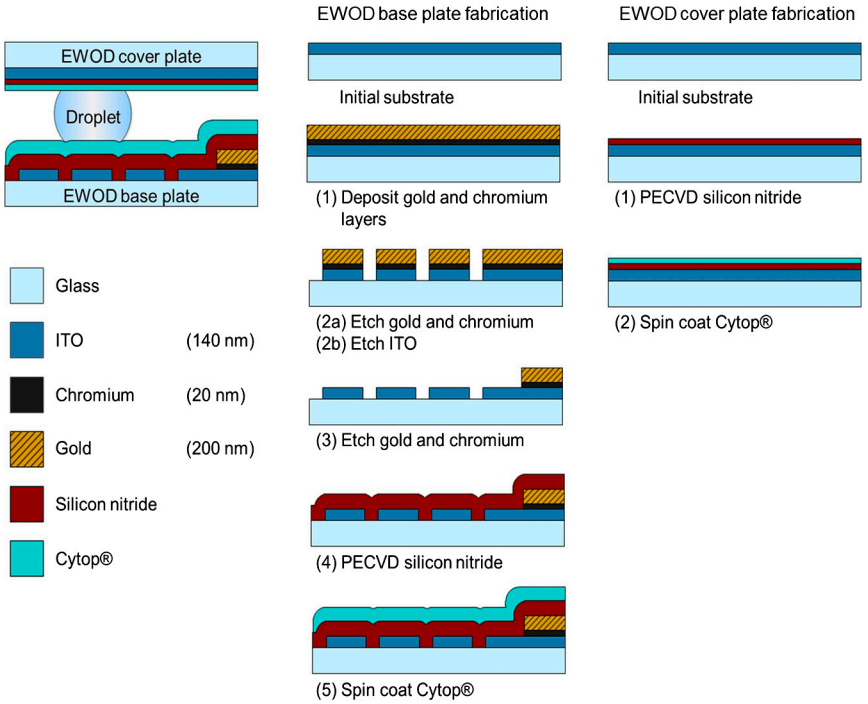

Fig. S1. (Left) Schematic of EWOD chip structure. (Center) Process flow to fabricate EWOD base plate. (Right) Process flow to fabricate EWOD cover plate. (Note: diagrams not to scale.)

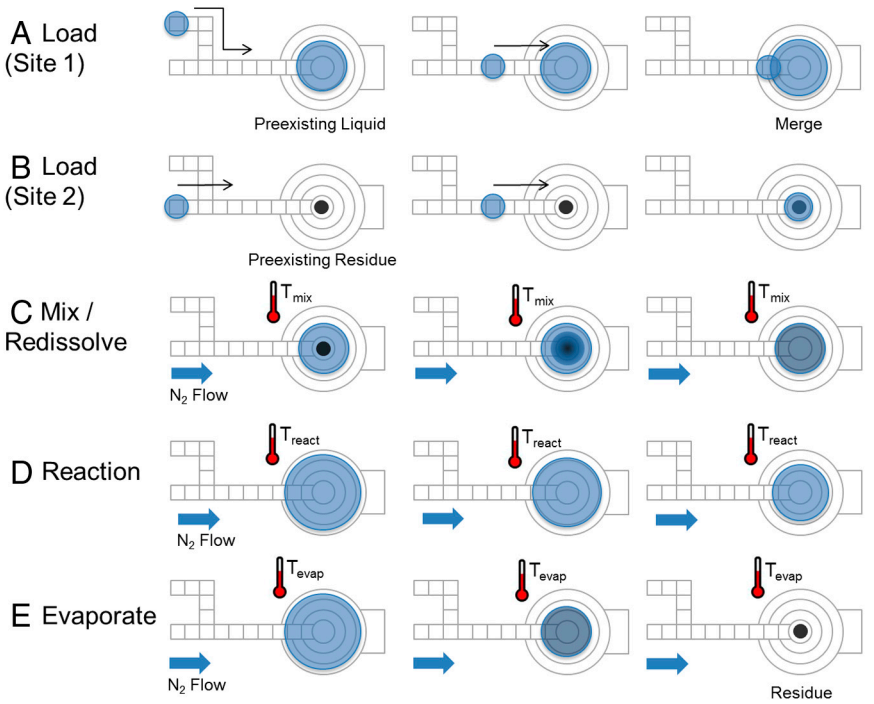

Fig. S2. Representative illustration of several chemical unit processes such as reagent loading, mixing, redissolving, reaction and evaporation on EWOD chip. Prior to a loading step, the heater may be empty, contain liquid (e.g., first row of images), or contain dried residue (e.g., second row of images). Black arrows indicate direction of droplet movement via EWOD to the reaction site (heater), while block blue arrows represent the direction of nitrogen flow. Nitrogen flow removes vapor during evaporation steps, but was also found to be effective in reaction steps and mixing to stabilize the droplet while heated near or above the boiling point. Activation of the heater is indicated by the thermometer symbol with adjacent temperature.

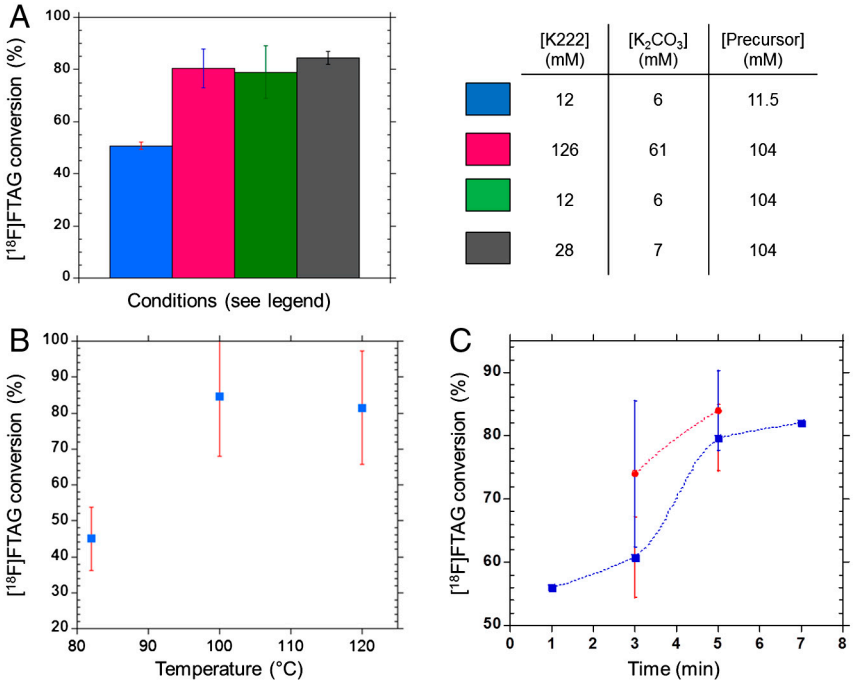

Fig. S3. (*A*) Effect of different concentrations of reagents on the efficiency of fluorination (of mannose triflate to produce [^{18}F]FTAG) on Cytop-glass in DMSO while the reaction temperature and reaction time remained constant at 90 °C and 5 min, respectively. (*B*) Effect of temperature on the fluorination efficiency in DMSO on Cytop-glass. (*C*) Kinetic plot of the fluorination efficiency versus reaction time for fluorination reactions performed at 100 °C (red circles), and 120 °C (blue squares). The dashed lines are smoothed curve fits to aid visualization.

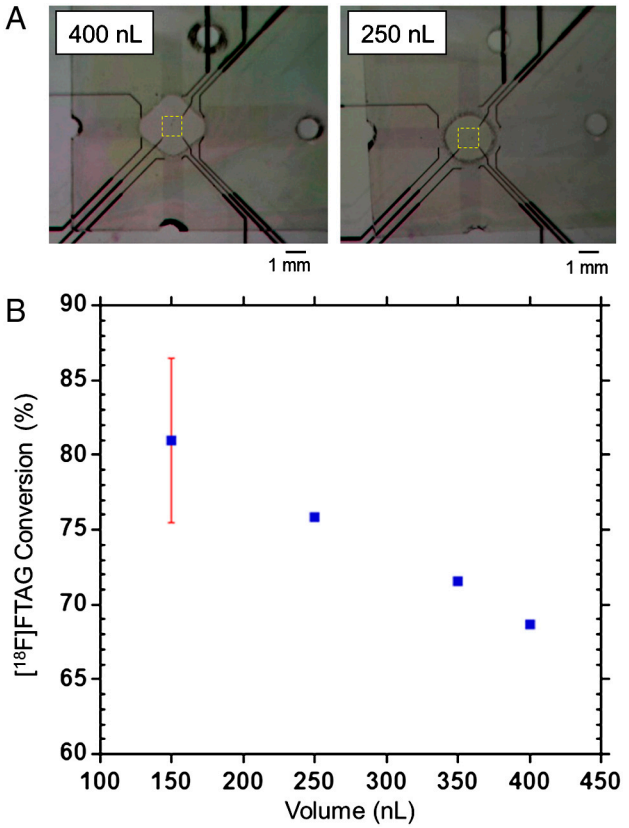

Fig. S4. (*A*) Digital photographs of two different droplet volumes greater than the heater size (heater is marked with a square dashed outline). (*B*) The effect on [^{18}F]FTAG conversion of the droplet volume.

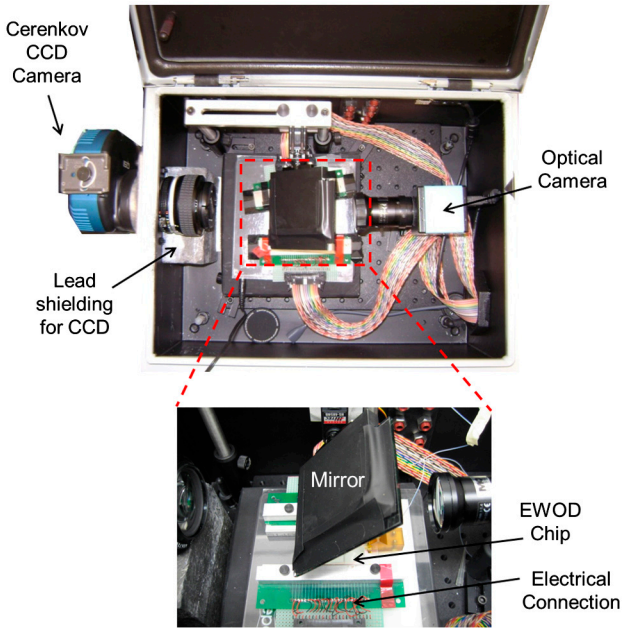

Fig. S5. (Top) Photograph looking down at the EWOD radiosynthesis chip set up inside the light-tight box of the Cerenkov imaging system. (Bottom) The EWOD chip is located underneath a pivoting mirror that can direct light to either the Cerenkov CCD (left) or optical imaging camera (right).

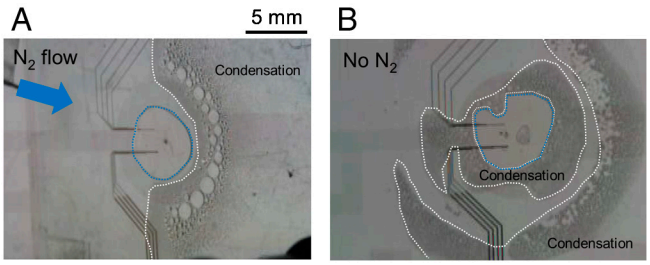

Fig. S6. Evaporation of the [^{18}F]KF/$K_{2.2.2}$ in MeCN and water mixture on EWOD (*A*) with the nitrogen flow as indicated by the blue arrow and (*B*) without nitrogen flow. The boundary of the liquid droplet is outlined in blue dashes and the boundaries of regions where vapor has recondensed (due to contact with cooler surfaces outside the heater site) are outlined in white dashes. With nitrogen flow, no condensation is observed on the upstream side of the droplet, suggesting that the flow is effective in removing vapor from that part of the chip. In the absence of the nitrogen flow, solvent vapor condensed all around the reaction site, and presumably slows further evaporation by maintaining high vapor pressure in the vicinity of the droplet-air surface.

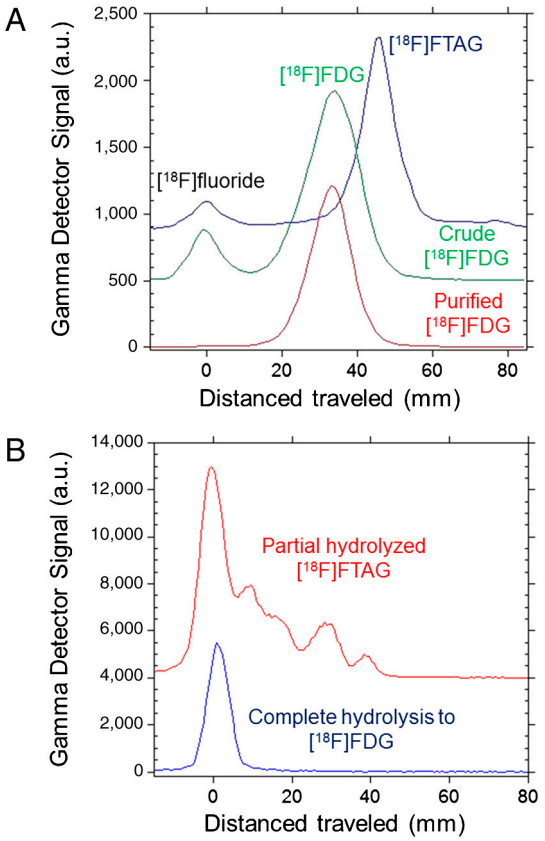

Fig. S7. (*A*) Representative radio-TLC of the crude [^{18}F]FTAG (green trace), the crude [^{18}F]FDG and the purified [^{18}F]FDG developed in 95:5 MeCN/H_2O (blue trace) with an average fluorination efficiency of 88 $\pm$ 7% ($n = 11$). The red trace showed that the purified [^{18}F]FDG had >99% radiochemical purity. (*B*) Radio-TLC of the crude reaction products developed in 50:50 hexane/ethyl acetate solvent mixtures to determine the extent of hydrolysis. The red radio-chromatogram showed partially hydrolyzed [^{18}F]FTAG obtained from an unoptimized hydrolysis condition, while the blue radio-chromatogram represented a fully hydrolyzed [^{18}F]FDG.

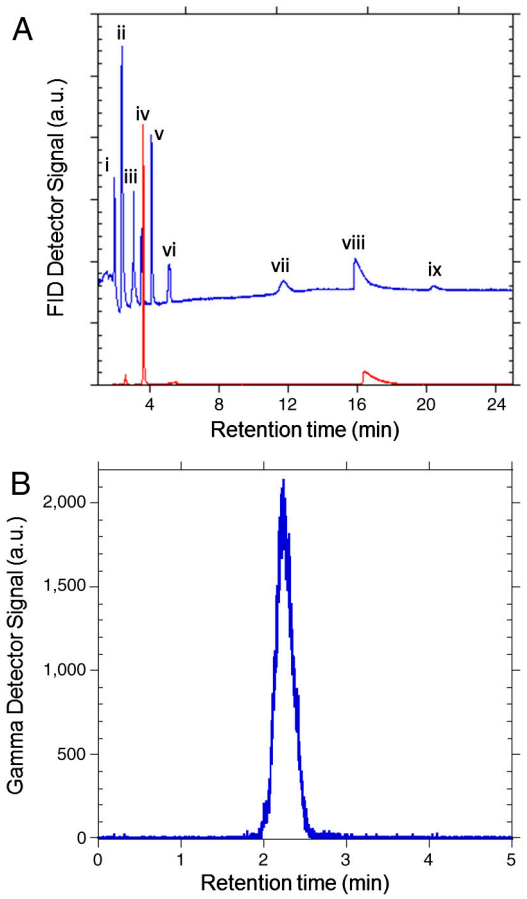

Fig. S8. (*A*) (Blue trace) Standards GC-FID chromatogram of mixtures of DMSO byproduct and residual solvents used in the preparation of [^{18}F]FDG. (Red trace) Representative chromatogram of [^{18}F]FDG prepared on EWOD. Peaks: (*i*) dimethyl sulfide, (*ii*) acetone, (*iii*) methanol, (*iv*) ethanol, (*v*) acetonitrile, (*vi*) methyl disulfide, (*vii*) bis(thiomethyl)methane, (*viii*) dimethyl sulfoxide, and (*ix*) dimethyl sulfone. (*B*) Representative radio-HPLC chromatogram of the purified [^{18}F]FDG using the miniaturized cartridge. Corresponding retention times are 1.96, 2.38, 3.0, 3.5, 4.1, 5.1, 11.7, 15.8, and 20.4 min.

Table S1. Comparison of several parameters of FDG synthesis on reported microfluidic platforms

	Batch	Batch	Batch	Flow-through	Flow-through
Reference	this work	1	2	3	4
Fluid path configuration	programmable	fixed	fixed	fixed	fixed
Solvent compatibility	excellent	poor	poor	limited	excellent
On-chip fluoride drying?	yes	yes	no (Note 1)	no	no
Precusor (μg)	200	0.3	125	25,000	40,000–45,000
Reaction volume (μL)	1–16 (Note 2)	0.04	5	200 (each reagent)	500 (each reagent)
FDG conversion efficiency (%) (Note 3)	88 ± 7%, $n = 11$	97.6%, $n = 1$	up to 96%, $n = ?$	>50%, $n = ?$	20%, $n = ?$
Total on-chip synthesis time (min) (Note 4)	60	14	14 + ? (off-chip drying time)	0.1 + ? (off-chip drying time)	10 +8 (off-chip drying time)
Performed purification (off-chip)?	yes (15 min)	No	yes (time = ?)	no	no
Final radiochemical purity (%)	>99	>90	>99	—	—
Highest reported on-chip starting radioactivity (mCi)	4.6	0.5	812	13.5	1-1,000
Highest reported final radioactivity (mCi)	0.7	0.19	3	—	—
Decay corrected radiochemical yield including purification (%)	22 ± 8%, $n = 11$	41.5%, $n = 1$ (Note 5)	—	—	—
Product passed QC tests? (color/clarity, solvents, pH, Kryptofix)	yes	—	—	—	—

[Notes (1): The chip is capable of on-chip fluoride drying, but, as described in the supporting information of ref. 2, off-chip drying was used for most of reported data due to chip reliability issues. (2): The concentric heater electode patterns permits different reaction volumes. (3): These values are obtained from radio-TLC of crude product after the radio-fluorination and hydrolysis reactions, without regard for radioactivity loss (e.g., fluoride) that may have occurred. (4): For flow-through chips, we report total reaction time, not the residence time. (5): Decay-correction applied to reported 38% radiochemical yield, assuming 14 min reported synthesis time. A dash in any entry means no data was reported]

1 Lee CC, et al. (2005) Multistep synthesis of a radiolabeled imaging probe using integrated microfluidics. *Science* 310:1793–1796.
2 Elizarov AM, et al. (2010) Design and optimization of coin-shaped microreactor chips for pet radiopharmaceutical synthesis. *J Nucl Med* 51:282–287.
3 Gillies JM, et al. (2006) Microfluidic technology for PET radiochemistry. *App Rad Isot* 64:333–336.
4 Steel CJ, et al. (2007) Automated PET radiosyntheses using microfluidic devices. *J Label Compd Radiopharm* 50:308–311.